

Dalton Transactions

Accepted Manuscript



This article can be cited before page numbers have been issued, to do this please use: S. Gahlot, E. Jeanneau, F. Dappozze, C. Guillard and S. Mishra, *Dalton Trans.*, 2018, DOI: 10.1039/C8DT01625A.



This is an Accepted Manuscript, which has been through the Royal Society of Chemistry peer review process and has been accepted for publication.

Accepted Manuscripts are published online shortly after acceptance, before technical editing, formatting and proof reading. Using this free service, authors can make their results available to the community, in citable form, before we publish the edited article. We will replace this Accepted Manuscript with the edited and formatted Advance Article as soon as it is available.

You can find more information about Accepted Manuscripts in the [author guidelines](#).

Please note that technical editing may introduce minor changes to the text and/or graphics, which may alter content. The journal's standard [Terms & Conditions](#) and the ethical guidelines, outlined in our [author and reviewer resource centre](#), still apply. In no event shall the Royal Society of Chemistry be held responsible for any errors or omissions in this Accepted Manuscript or any consequences arising from the use of any information it contains.

Cite this: DOI: 10.1039/c0xx00000x

www.rsc.org/xxxxxx

ARTICLE TYPE

Precursor-mediated synthesis of Cu_{2-x}Se nanoparticles and its composites with TiO_2 for improved photocatalysis†

Sweta Gahlot,^a Erwann Jeanneau,^b Frederic Dappozze,^a Chantal Guillard,^a and Shashank Mishra^{*a}

Received (in XXX, XXX) Xth XXXXXXXXX 20XX, Accepted Xth XXXXXXXXX 20XX

DOI: 10.1039/b000000x

Direct synthesis of copper selenide nanoparticles from the reaction of ditertiarybutyl selenide $t\text{Bu}_2\text{Se}$ with copper(II) trifluoroacetate $\text{Cu}(\text{TFA})_2$ under mild conditions is reported. Isolation of a molecular species during the course of this reaction, established as $[\text{Cu}_2(\text{TFA})_2(t\text{Bu}_2\text{Se})_3]$ by spectroscopic studies and single crystal X-ray structure, confirmed that metal selenide NPs are formed *via* this intermediate species containing reduced copper center. Extending this reaction in the presence of commercial TiO_2 (P25) offered an easy synthesis of copper selenide-titania nanocomposites with different Cu/Ti ratios. These nanocomposites, well-characterized by powder XRD, STEM, TEM, BET, XPS, EDX and UV-Vis studies, were examined as photocatalysts for the degradation of formic acid (FA). The $n\text{Cu}_{2-x}\text{Se-TiO}_2$ nanocomposites with low mol% of copper selenide i.e., $n = 0.1$ and 0.3 mol%, displayed a superior catalytic activity over P25, which is an established benchmark for the photocatalysis under UV light.

Introduction

Excellent physical and chemical properties of well-known semiconducting photocatalyst TiO_2 make it stand out from the other photocatalysts. However, its low photonic efficiency in the visible region and fast recombination of a large population of photo generated electron-hole pairs are major limitations for its application in photocatalytic process.¹ Among many strategies to improve the photocatalytic efficiency of TiO_2 , a majority of which includes introduction of metallic or non-metallic impurity inside to modify its electronic structure, one effective method is to combine it with another low bandgap semiconducting materials to extend its absorption spectrum and to sensitize it for UV-vis-driven photocatalysis.² Some examples of metal-chalcogenide based semiconducting materials used for this purpose are CdS ,³ CdSe ,⁴ CdSeTe ,⁵ Ag_2S ,⁶ and Ag_2Se .⁷ An earlier work from this laboratory has shown a ‘bottom-up’ synthesis of $\text{Ag}_2\text{Se-TiO}_2$ nanocomposites which exhibited better catalytic activity as compared to the commercially available TiO_2 (P25).⁷ Though an improved photocatalyst, the composite $\text{Ag}_2\text{Se-TiO}_2$ suffered a drawback of being photosensitive in nature that caused the degradation of Ag_2Se to Ag nanoparticles on prolonged exposure to light. Further, silver raises concerns over its adverse effects on health and environment. These limitations, coupled with silver’s high costs, prompted us to consider copper selenide as an efficient alternative to above nanocomposites. To the best of our knowledge, there is no report on the photocatalysis of $\text{Cu}_{2-x}\text{Se-TiO}_2$ composites, though Chen *et al.* recently reported the preparation of complex $\text{Cu}_2\text{Se-CdSe-TiO}_2$ composites which showed many fold enhancement in photocurrent density as compared to pure TiO_2 .⁸

Copper selenide is a p-type semiconductor which exists in

multiple structural forms such as tetragonal umangite (Cu_3Se_2), cubic berzelianite (Cu_2Se , $\text{Cu}_{1.8}\text{Se}$), orthorhombic marcasite (CuSe_2), orthorhombic atabascite (Cu_5Se_4) and hexagonal klockmannite (CuSe , $\text{Cu}_{0.87}\text{Se}$).⁹ In addition, its atomic rearrangement in binary non-stoichiometric Cu_{2-x}Se is quite complex, and a wide variety of crystal phases with diverse defects exist.¹⁰ Cu_{2-x}Se crystals show high conversion efficiency as their bandgaps lie in the range of 1.4–2.2 eV. Several chemical routes have been employed for the synthesis of controlled morphologies of copper selenide nanostructures with size ranging in a broad spectrum.^{10–16} These include i) solvothermal process using either sodium selenite/copper acetate/ethylene glycol-water,¹⁰ or Se powder/Cu foil/hexanol,¹¹ ii) hydrothermal method using ionic liquid as selenium source,¹² iii) template method using preformed CuO ,¹³ iv) redox reaction using copper sulphate/Se NPs/polystyrene sulfonate,¹⁴ v) one-pot synthesis using copper stearate/Se-octadecene/oleic acid-oleylamine,¹⁵ and vi) hot injection method using $\text{CuCl/Ph}_2\text{Se}_2/1\text{-octadecene-oleylamine}$.¹⁶ Bottom-up synthesis of nanomaterials using well-defined molecular precursors offers numerous advantages over other synthetic routes.¹⁷ However, thoroughly characterized single source precursors (SSPs) for copper selenide nanomaterials are limited and a majority of them require high temperatures for their conversion into nanomaterials.¹⁸ Recently, selenoethers have emerged as simple yet effective sources of producing selenium-containing chalcopyrite semiconducting materials.^{19,20} Several researchers have used metal complexes with selenoethers as single source precursors,¹⁹ while others have employed the reactions of selenoethers R_2Se ($\text{R} = \text{Me}$, Et , $t\text{Bu}$) with metal halides, metal oxohalides and metal alkyls in chemical vapor deposition (CVD) technique to derive high-quality metal solenoid films.²⁰ With an aim to develop new and effective precursors for

copper selenide nanomaterials, we studied the reactions of selenoether with different copper reagents. While the reaction of ditertiarybutyl selenide $t\text{Bu}_2\text{Se}$ with $\text{Cu}(\text{TFA})_2$ (TFA = trifluoroacetate) in various solvents resulted in the formation of Cu_{2-x}Se NPs under mild conditions, its reaction with CuI led to isolation of a stable molecular complex $[\text{Cu}_4\text{I}_4(t\text{Bu}_2\text{Se})_4]$. Successful isolation of a molecular species in the former case, established as $[\text{Cu}_2(\text{TFA})_2(t\text{Bu}_2\text{Se})_3]$ by spectroscopic studies and single crystal X-ray structure, confirmed that copper selenide NPs are formed *via* this intermediate species containing reduced copper center. Although several families of molecular precursors are known for metal chalcogenide nanomaterials,²¹ except for one publication from our group,⁷ there is no report available in the literature on the use of selenoether ligand in Chemical Solution Deposition (CSD) of metal selenides. The compounds reported here assume importance because not only they satisfy the general criteria of CSD precursors such as easy preparation, good solubility in organic solvents, and facile and clean decomposition but also highlight the dual role of the selenoether i.e., a facile source of selenium and a reducing reagent to get desirable +1 oxidation state of the copper center. Equally important is the fact that a well-defined chemical route for the formation of copper selenide nanoparticles is unequivocally established here by the isolation and complete characterization of the intermediate $[\text{Cu}_2(\text{TFA})_2(t\text{Bu}_2\text{Se})_3]$. After thoroughly characterizing the intermediate and final complexes and establishing the route for their conversion to nanoparticles, we proceeded further to obtain copper selenide-titania nanocomposites that showed an improved photocatalytic activity over the commercial TiO_2 (P25) for the degradation of formic acid (FA) solution on UV irradiation. The photodegradation of formic acid was selected as a model reaction because not only it is converted to CO_2 and H_2O without the formation of any stable intermediate species, but the reaction also represents a possible final step in the photodegradation of more complex organic compounds.²² The P25 is considered a benchmark for photocatalytic reactions under UV-lights, and only a few studies have reported a superior photocatalytic activity.

Experimental

General Procedures. Except for photocatalysis, which was carried under ambient atmosphere, all other manipulations were performed under the argon atmosphere using standard Schlenk and glovebox techniques. Solvents were dried using MB SPS-800 and used without further purification. Copper(II) trifluoroacetate and copper(I) iodide (both Aldrich), di-tertiary-butylselenide $t\text{Bu}_2\text{Se}$ (SAFC Hitech), TiO_2 (P25, Evonik, ex-Degussa) and formic acid (99%, Acros Organics) were purchased and used without further purification. ^1H NMR spectra were recorded in CDCl_3 on a Bruker AC-300 spectrometer. The infrared spectra were obtained as Nujol mulls on a Bruker Vector 22 FT-IR spectrometer at room temperature and registered from 4000 to 400 cm^{-1} . The scanning electron microscopy (SEM) measurements were performed on Hitachi S800. TEM experiments were performed using a JEM-2100F with 200kV field emission (FE) and JEOL 2010 LaB6 with 200kV FE. We used a Bruker D8 Advance A25 with $\text{Cu K}\alpha 1+2$ ($\lambda=0.154184$

nm) radiation at 50 kV and 35 mA to measure the X-ray diffraction (XRD) patterns of the powdered crystals. The absorbance characteristics of the nanocomposites were measured using a UV-vis spectrophotometer (AvaSpec Avantes Fiber Optic Spectrometer systems). The nitrogen adsorption and desorption isotherms were measured on an ASAP 2020 system. We employed the linear part of Brunauer-Emmett-Teller (BET) method to calculate the specific surface area of these nanocomposites, while Barrett-Joyner-Halenda (BJH) method provided their pore size distribution. An electron spectrometer (Kratos Axis Ultra DLD) with an $\text{Al K}\alpha$ (1486.6 eV) radiation source was used to perform the X-ray photoelectron spectroscopy (XPS) analysis of the catalysts. Corrections on the constant charging of the XPS spectra were made by C 1s of adventitious carbon (binding energy of 284.6 eV).

Synthesis of copper complexes and Cu_{2-x}Se nanoparticles

$[\text{Cu}_2(\text{TFA})_2(t\text{Bu}_2\text{Se})_3]$ (1). $t\text{Bu}_2\text{Se}$ (0.062 mL, 0.32 mmol) was added dropwise to the blue colored solution of $\text{Cu}(\text{TFA})_2$ (0.1 g, 0.32 mmol). After stirring the solution for 15 minutes at room temperature, the solution was concentrated under vacuum and layered with *n*-pentane to obtain colorless crystals of **1**. Crystals were isolated after removing the mother liquor through cannula, followed by subsequent washing with cold *n*-pentane. Yield, 1.0 g (60%). FT-IR (nujol, cm^{-1}): 3120w, 3075w, 2722w, 2376w, 1685s, 1461s, 1370s, 1207s, 1143s, 1017m, 926w, 835s, 790m, 718s, 609w, 527m. ^1H NMR (CDCl_3 , 23°C, ppm): δ 1.58.

$[\text{Cu}_4\text{I}_4(t\text{Bu}_2\text{Se})_4]$ (2). A dichloromethane solution containing CuI (0.1 g, 0.52 mmol) and $t\text{Bu}_2\text{Se}$ (0.15 mL, 0.78 mmol) was stirred at room temperature for 1 hour. Colorless crystals of **2** were obtained from the concentrated solution at -10°C . The crystallized product was isolated after removing the mother solution through cannula, followed by subsequent washing with cold *n*-pentane. Yield, 0.16 g (78%). Anal.: calcd for $\text{C}_{32}\text{H}_{72}\text{Cu}_4\text{I}_4\text{Se}_4$ (1534.4): C, 25.0, H, 4.69; found: C, 24.4, H, 4.61%. FT-IR (nujol, cm^{-1}): 2990s-2860s, 1472s, 1400m, 1390s, 1364s, 1210m, 1155s, 1025m, 930w, 810, 610w. ^1H NMR (CDCl_3 , 23°C, ppm): δ 1.55.

Cu_{2-x}Se nanoparticles. We optimized the conditions for the preparation of Cu_{2-x}Se NPs by varying the reactants, solvents, temperature and stirring/refluxing time of the reactions (*vide infra*, results & discussion section). Stirring of a reaction mixture containing $\text{Cu}(\text{TFA})_2$ (0.12 g, 0.34 mmol) and $t\text{Bu}_2\text{Se}$ (0.04 mL, 0.20 mmol) in Et_2O (20 mL) led to gradual change of the color of the solution, from blue to green and then brown. Further stirring of this reaction mixture for 24 h afforded black coloured nanoparticles of Cu_{2-x}Se . The reaction time could be reduced to 3 hours by refluxing the THF (30 mL) solution containing $\text{Cu}(\text{TFA})_2$ (0.1 g, 0.28 mmol) and $t\text{Bu}_2\text{Se}$ (0.03 mL, 0.17 mmol) at 65 °C, though the yield was quite poor (~10%). The yield of Cu_{2-x}Se NPs, however, could be enhanced significantly up to 94% by substituting the solvent THF with toluene and refluxing the mixture at 115 °C for 3 h.

Preparation of *n*% $\text{Cu}_{2-x}\text{Se-TiO}_2$ nanocomposites

0.1%Cu_{2-x}Se-TiO₂. Cu(TFA)₂ (0.006 g, 0.017 mmol) was stirred in toluene (20 mL) for 15 min to get a transparent light blue solution. After adding TiO₂ (P25) (0.7 g, 8.76 mmol) and stirring the reaction mixture for 15 min, an excess of ¹Bu₂Se was added dropwise. The obtained mixture was refluxed for 3 h after which an off-white powder was isolated by centrifugation. The powder was then washed with ethanol several times and dried at room temperature.

Using above method, 0.3%Cu_{2-x}Se-TiO₂ and 1% Cu_{2-x}Se-TiO₂ nanocomposites were also synthesized using appropriate ratios of Cu(TFA)₂, ¹Bu₂Se and TiO₂.

Formic Acid Photodegradation. Nanocomposite powder (30 mg) was dispersed in 30 mL aqueous solution of 50 ppm formic acid. The suspension was magnetically stirred for 30 min in the dark to obtain a complete adsorption-desorption equilibrium. It was then irradiated with UV-Vis lamp (HPK 125 W high-pressure mercury vapor lamp). A cutoff filter with $\lambda > 350$ nm placed in a water cuvette situated beneath the reactor was used to perform the photocatalytic degradations of FA. The cutoff filter allows the use of wavelength at 365 nm only. We measured the radiant flux using a VLX-3W radiometer with a CX-365 detector (UV-A). The distance between the photoreactor and the water cell was controlled to maintain the radiant flux fixed at 4.1 ± 0.2 mWcm⁻² for all photocatalytic tests. The concentration of formic acid was determined by HPLC, with VARIAN Star Series, with ICE COREGEL 87-H3 (300x7.8mm), a Star-230 pump, a Star-325 UV-Vis detector detecting at 210nm and a Star-410 autosampler. The mobile phase consisted of 5×10^{-3} mol/L of H₂SO₄ (pH2) with a flow rate of 0.7 ml/min, while the Column thermostat is set at 30 °C. Photodegradation under visible light was performed using visible LED (white light) lamps manufactured by Macrolenses (Germany). After stirring in the dark for 30 min, a 30 mL FA (50 ppm) solution containing 30 mg of catalyst was irradiated under visible light for 3 h.

X-Ray Crystallography. Suitable crystals of **1** and **2** were obtained as described in the synthetic procedure. Crystal structure were measured using Mo radiation ($\lambda = 0.71073$ Å) on an Oxford Diffraction Gemini diffractometer equipped with an Atlas CCD detector. Intensities were collected at 100 K by means of the CrysAlisPro software.²³ Reflection indexing, unit-cell parameters refinement, Lorentz-polarization correction, peak integration and background determination were carried out with the CrysAlisPro software.²³ An analytical absorption correction was applied using the modeled faces of the crystal.²⁴ The resulting sets of hkl were used for structure solutions and refinements. The structures were solved by direct methods with SIR97²⁵ and the least-square refinement on F2 was achieved with the CRYSTALS software.²⁶

Crystallographic and refinement data. [Cu₂(TFA)₂(¹Bu₂Se)₃] (**1**): Mr = 932.69, Triclinic, *P*-1, *a* = 12.0827(6) Å, *b* = 16.2379(9) Å, *c* = 20.2592(10) Å, α = 91.486(4)°, β = 92.316(4)°, γ = 104.996(5)°, *V* = 3833.6(4) Å³, *Z* = 4, μ = 4.02 mm⁻¹, *T* = 150 K, 69037 Measured reflections, 19642 Independent reflections, *R*_{int} = 0.056, 19600 no. of reflections, 63 restraints, 775 parameters, *S* = 1.01, $R[F^2 > 2\sigma(F^2)] = 0.072$, $wR(F^2) = 0.150$,

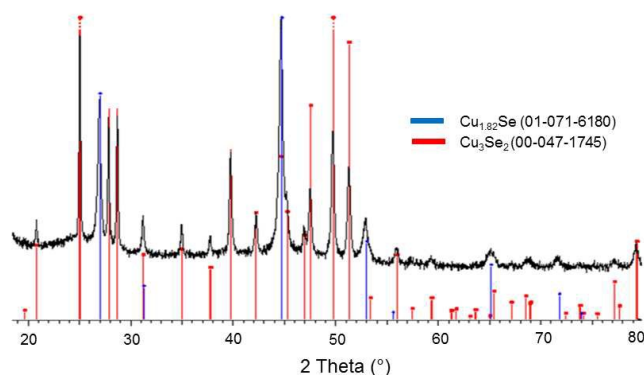


Figure 1. XRD pattern of Cu_{2-x}Se NPs obtained from the reaction of Cu(TFA)₂ and ¹Bu₂Se in toluene under refluxing condition.

$\Delta\rho_{\max} = 2.38 \text{ e.}\text{\AA}^{-3}$, $\Delta\rho_{\min} = -1.89 \text{ e.}\text{\AA}^{-3}$. [Cu₄I₄(¹Bu₂Se)₄] (**2**): Mr = 1534.5, Monoclinic, *Cc*, *a* = 14.7484(4) Å, *b* = 14.7713(3) Å, *c* = 22.8613(7) Å, β = 97.390(3)°, *V* = 4939.0(2) Å³, *Z* = 4, μ = 7.17 mm⁻¹, *T* = 150 K, 21683 Measured reflections, 10065 Independent reflections, *R*_{int} = 0.069, 9995 no. of reflections, 274 restraints, 398 parameters, *S* = 0.97, $R[F^2 > 2\sigma(F^2)] = 0.113$, $wR(F^2) = 0.237$, $\Delta\rho_{\max} = 4.50 \text{ e.}\text{\AA}^{-3}$, $\Delta\rho_{\min} = -2.74 \text{ e.}\text{\AA}^{-3}$.

Results and discussions

(a) Divergent reactivity of ¹Bu₂Se with copper reagents: Formation of Cu_{2-x}Se nanoparticles vs. molecular complex

Extending our previous work on the reactivity of selenoethers with silver(I) reagent,⁷ we studied here the reactions of ¹Bu₂Se with two different copper reagents *i.e.*, Cu(TFA)₂ (where TFA = trifluoroacetate) and CuI in different solvents. The aim was to exploit the divergent reactivity of above selenoether to obtain copper selenide nanomaterials and its composites with TiO₂ for photocatalytic applications. Addition of ¹Bu₂Se to Cu(TFA)₂ at room temperature in a variety of solvents (diethylether, tetrahydrofuran or toluene) led to gradual change in color of the solution from blue to green and finally precipitation of a black colored copper selenide powder, as determined by powder X-ray diffraction studies (Fig. S1). However, reactions at room temperature were not very reproducible in terms of yield and time needed for precipitation (varied from few hours to one or two days) and sometimes, there were unrecognised impurities (extra peaks in XRD which we could not index). However, by performing the reactions under refluxing conditions, we not only reduced the reaction time significantly, but also made it reproducible in terms of products obtained. Thus, the color of the THF solution, on refluxing at 65 °C, changed from dark green to brown and then to black to give finally black precipitate after 3 hours (albeit in low yield of 10%). The powder XRD of this precipitate indicated it to be a mixture of two phases of copper selenide Cu_{1.82}Se (01-071-6180) and Cu₃Se₂ (00-047-1745) (Fig. S2). We succeeded to increasing the yield of nanoparticles significantly by taking toluene as a solvent and refluxing the reaction mixture at a raised temperature of 115 °C. These reaction conditions were reproducible which always led to the formation of Cu_{1.82}Se as a major phase (in addition to Cu₃Se₂ as a minor phase) (Fig. 1). Refluxing in toluene, however, increased the average size of nanoparticles to 55 nm from 20 nm as determined using the Debye-Scherrer formula. The SEM images show

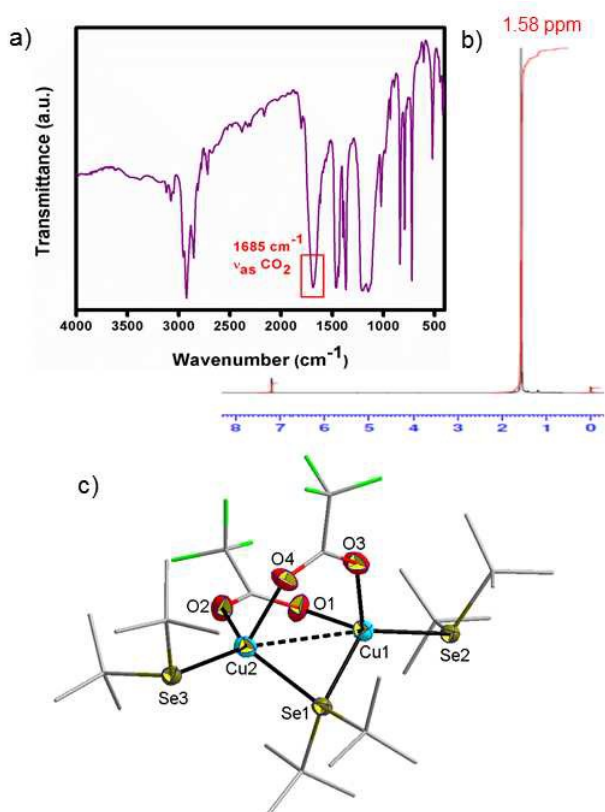


Figure 2. Characterization of the intermediate species $[\text{Cu}_2(\text{TFA})_2(\text{Bu}_2\text{Se})_3]$ (**1**). (a) FT-IR spectrum, (b) ^1H NMR spectrum, and (c) perspective view of the molecular structure with 50% probability ellipsoids (H atoms omitted for clarity). Selected bond lengths (Å) and angles ($^\circ$): Cu1—O1 2.061(6), Cu1—O3 2.078(6), Cu2—O2 2.065(6), Cu1—Se1 2.437(1), Cu2—Se1 2.432(1), Cu1—Se2 2.365(1), Cu2—Se3 2.360(1), Cu1 \cdots Cu2 3.408(1), O1—Cu1—O3 95.0(3), Se1—Cu1—O3 100.8(2), Se2—Cu1—O3 115.3(2), Cu1—Cu2—Se3 168.3(5).

significant aggregation of these particles (Fig. S3), which is not surprising given that the synthesis was achieved in the absence of any capping ligand. The gradual change in the color of $\text{Cu}(\text{TFA})_2$ solution on adding Bu_2Se suggested that the copper selenide nanoparticles are formed *via* the reduction of copper(II) species. Therefore, attempts were made to characterize the species present in the solution before the precipitation of Cu_{2-x}Se NPs. We succeeded in isolating an intermediate molecular species $[\text{Cu}_2(\text{TFA})_2(\text{Bu}_2\text{Se})_3]$ (**1**) from the reaction mixture and characterising it by spectroscopic and single crystal X-ray diffraction studies (Fig. 2), which showed that the copper center in this complex are in +1 oxidation state (*vide infra*). The ability of selenoethers to reduce metal centers has previously been demonstrated.²⁷ In contrast to above observation, the reaction of Bu_2Se with copper iodide in dichloromethane was straight forward, which led to the isolation of a stable molecular complex $[\text{Cu}_4\text{I}_4(\text{Bu}_2\text{Se})_4]$ (**2**). Unlike the intermediate derivative **1**, which turns gradually black even when kept in dark at low temperature and under inert atmosphere, apparently due to the formation of Cu_{2-x}Se NPs, complex **2** is stable at rt. Fortunately, the intermediate **1** was stable for sufficiently long time to allow its complete characterization. This complex is also more soluble in common organic solvent as compared to **2** which is soluble in dichloromethane but shows limited to poor solubility in other

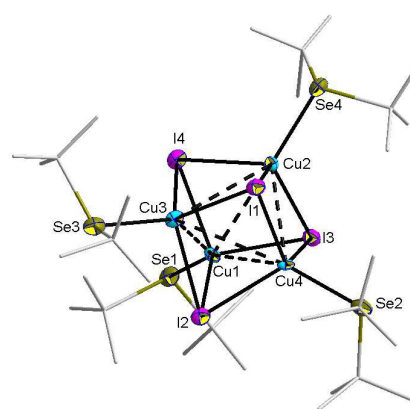


Figure 3. Perspective view of the molecular structures of **2** with 50% probability ellipsoids. H atoms on alkyl group are omitted for clarity. Selected bond lengths (Å) and angles ($^\circ$): I1—Cu1 2.783(4), I1—Cu2 2.728(3), I2—Cu1 2.706(4), Cu1 \cdots Cu2 2.997(4), Cu1 \cdots Cu4 3.287(4), Cu3 \cdots Cu4 3.001(4), Cu1—Se1 2.452(4), Cu2—Se2 2.470(5), I1—Cu1—Se1 102.3(1), I1—Cu1—I3 100.9(1), I2—Cu3—I4 104.8(1).

solvents (THF, toluene, hexane). The high reactivity of Bu_2Se to give directly metal selenide nanoparticles could be attributed to availability of a decomposition path *via* β -hydrogen elimination as well as a weaker C-Se bond in this ligand.²⁸ Among copper reagents used here, the trifluoroacetate (TFA) ligand appears to be more labile than the iodide ligand. Such a trend was observed previously also.^{7,29} It is pertinent to note that only few well-characterized coordination complexes of copper with the neutral selenide-containing ligands exist in the literature.³⁰

The FT-IR spectra of **1** and **2** show characteristic bands for the ligand Bu_2Se , the former complex also showing additional bands for the trifluoroacetate ligand (Fig. 2a). Presence of only one strong band due to $\nu_{\text{as}}\text{CO}_2$ at 1685 cm^{-1} is consistent with the fact that there is only one bonding mode of the TFA ligands in **1** (Fig. 2c). Other characteristic absorptions due to $\nu\text{C-F}$ and $\nu\text{C-O}$ of the TFA ligand as well as $\nu\text{Cu-O}$ vibrations are observed in the expected region.³¹ The ^1H NMR spectra of **1** and **2** in CDCl_3 are simple and show only a singlet at $\delta = 1.55\text{--}1.58\text{ ppm}$ for the Bu group of the selenoether (Fig. 2b). Complex **1** crystallizes in the triclinic space group $P-1$ (with $R = 0.072$ and $wR = 0.150$) and has two independent molecules in the asymmetric unit. Each molecule adopts a discrete dinuclear structure, where two copper(I) centers having a short cuperophilic interaction ($\text{Cu}\cdots\text{Cu} = 3.408(1)\text{--}3.417(1)\text{ \AA}$)³² are further bridged by one μ - Bu_2Se and two μ - η^1 : η^1 -TFA ligands (Fig. 2c). One terminal Bu_2Se on each copper atom then complete the pseudo-tetrahedral geometry around it (if $\text{Cu}\cdots\text{Cu}$ interaction is not taken into account), as indicated by the O-Cu-O, Se-Cu-Se and Se-Cu-O angles, which lie in the range $95.0(3)\text{--}124.6(5)$. The Cu- μ -Se bond distances [$2.431(1)\text{--}2.437(1)\text{ \AA}$] are longer than the terminal Cu-Se ones [$2.359(1)\text{--}2.374(1)\text{ \AA}$]. Such a trend has been observed previously also in the related copper halide clusters with thioethers.³³ The Cu-O bond lengths, $2.052(6)\text{--}2.079(6)\text{ \AA}$, for bridging trifluoroacetate ligand compare well with the literature values.³⁴ The tetrameric structure of $[\text{Cu}_4\text{I}_4(\text{Bu}_2\text{Se})_4]$ (**2**), which crystallizes in the monoclinic space group Cc (with $R = 0.113$ and $wR = 0.237$), is similar to that reported for its silver analogue.⁷ It presents a cubane geometry formed by four copper and four iodine atoms, which alternatively occupy the corners of a distorted cube, with the Bu_2Se ligands coordinated to the copper

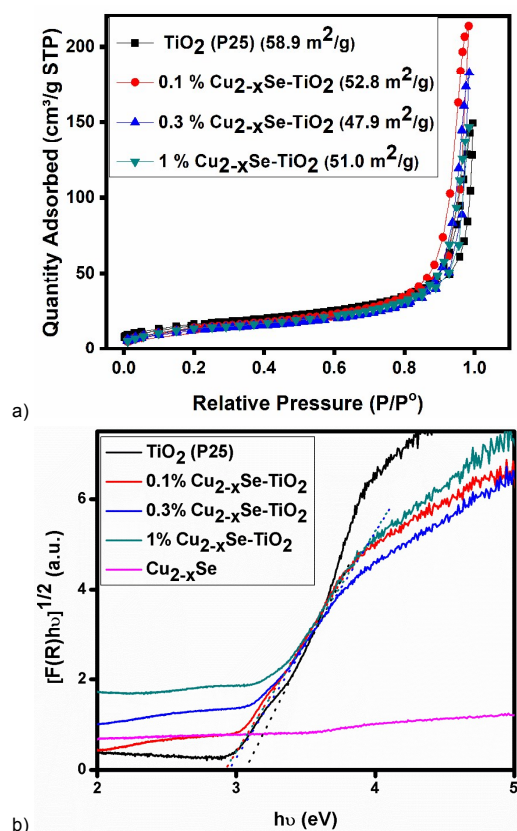


Figure 4. BET isotherms (a) and Kubelka munk plots (b) of P25 and $\text{Cu}_{2-x}\text{Se-TiO}_2$ nanocomposites with different % of Cu_{2-x}Se .

atoms (Fig. 3). Each face is distorted due to cuperophilic $\text{Cu}\cdots\text{Cu}$ interactions [2.997(4)-3.287(4) Å].³² The Cu-I [2.706(4)-2.805(4) Å] and Cu-Se [2.452(4)-2.470(5) Å] bond lengths in **2** are consistent with the literature value on related copper systems with bridging iodide and terminal bonded selenium containing ligands.³⁵ These cubanes are discrete entity and have no intermolecular interaction among them. This is different from the previously reported copper halide clusters with thioethers where cubane-like clusters [$\text{Cu}_4\text{I}_4(\text{Et}_2\text{S})_4$] act as secondary building units to give 1D coordination polymer.³³

(b) Preparation and characterization of $\text{Cu}_{2-x}\text{Se-TiO}_2$ nanocomposites

We prepared $n\text{Cu}_{2-x}\text{Se-TiO}_2$ nanocomposites with different Cu/Ti ratios ($n = 0.1, 0.3$ and 1 mol%) by refluxing $\text{Cu}(\text{TFA})_2$ and $n\text{Bu}_2\text{Se}$ in toluene with different amounts of commercial TiO_2 -P25. After general workup, the precipitated off-white powders were isolated through centrifugation, washed with ethanol and left to dry at room temperature for 24h (schematic representation in Fig. S4). Because of the low percentage of copper selenide content in these nanocomposites, their XRD patterns showed majorly the characteristic peaks of the commercial TiO_2 (P25) [00-021-1272 (anatase) and 01-079-6029 (rutile)] (Fig. S5). The surface characteristic of the commercial P25 and $n\text{Cu}_{2-x}\text{Se-TiO}_2$ nanocomposites were studied by Brunauer-Emmett-Teller (BET) measurements (Fig. 4a). The obtained isotherms are identified as type IV having small hysteresis loop in a relative pressure of 0.85-1.00. Compared to the pure TiO_2 , the nanocomposites showed a slight decrease in the BET surface area. Table S1

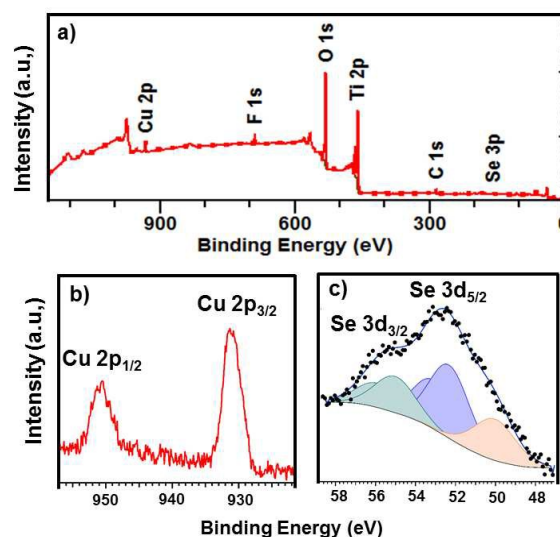


Figure 5. XPS spectra showing wide scan spectrum (a) and binding energies of Cu2p (b) and Se3d (c).

provides the surface areas, total pore volumes, and average pore diameters. We measured the band gap of the $n\text{Cu}_{2-x}\text{Se-TiO}_2$ nanocomposites (having different Cu/Ti ratios) through Kubelka munk plots as shown in Fig. 4b. TiO_2 shows the characteristic spectrum indicating a band gap of about 3.2 eV. However, as mol% of Cu_{2-x}Se increased, the band edge was red-shifted considerably (band gap in the region 3.1-2.9 eV) (Fig. S6). The increase in absorption is attributed to the narrow band gap of Cu_{2-x}Se NPs. With an increased absorption in the visible wavelength, more electron-hole pairs are expected to be generated in the composite under UV-Visible light. To further confirm the composition and valence state of these nanocomposites, X-ray photoelectron spectroscopy (XPS) studies were conducted on a representative sample $\text{Cu}_{2-x}\text{Se-TiO}_2$ with a copper selenide loading content of 1mol%. As shown in Fig. 5a, the wide scan spectrum indicates that this sample consists of the elements Ti, Cu, Se, O, C and F, the presence of the last element could be attributed to the use of copper trifluoroacetate as a starting reagent. The signal due to fluoride contamination, however, disappears in the recycled catalyst, indicating that the fluoride ions are adsorbed on the surface only. In the core level spectrum of the Ti 2p region, binding energies at 458.4 eV and 464.3 eV, corresponding to Ti 2p_{3/2} and Ti 2p_{1/2}, respectively, indicate the presence of Ti(IV) in the form of TiO_2 . The O 1s peak observed at 529.6 eV is attributed to the Ti-O-Ti bond, thus supporting the presence of TiO_2 .⁶ The observed peaks for Cu 2p_{3/2} and Cu 2p_{1/2} at 933 eV and 953 eV, respectively, and the lack of satellite peaks indicate the presence of copper in +1 oxidation state (Fig. 5b).³⁶ The Se 3d spectrum is deconvoluted to show the presence of two well-resolved doublets (Fig. 5c), the major peak located at 52.3 eV and corresponding to Se 3d_{5/2}, indicates Se^{2-} ,³⁷ though a very small contribution due to metallic selenium is also observed at about 50 eV. The presence of trace amount of metallic selenium in the precursor-directed synthesis was observed previously also.⁷ We are currently working on to address it by varying the experimental conditions. The microstructures and the morphology of this representative composite were further studied

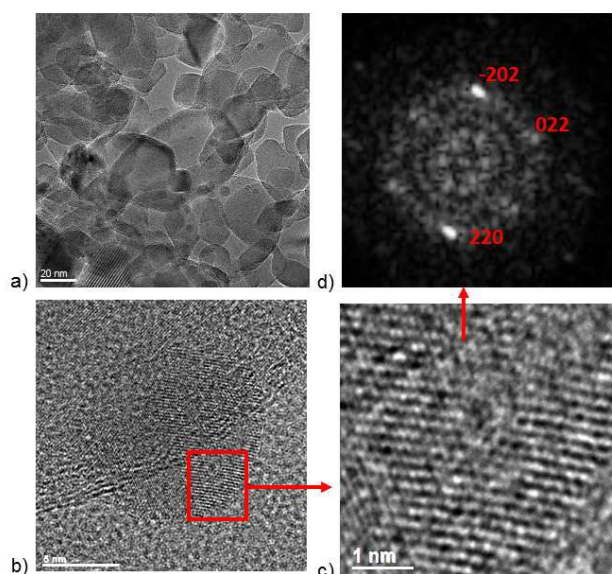


Figure 6. TEM and HR-TEM images of 1% $\text{Cu}_{2-x}\text{Se-TiO}_2$ nanocomposite at different resolution (a-c). Fig. S5d shows selected area diffraction pattern of Cu_{2-x}Se NPs.

by STEM and HR-TEM studies (Fig. 6, S7 and S8). While STEM images indicated intimate mixing of the TiO_2 and Cu_{2-x}Se components, the EDX spectra confirmed the presence of Cu and Se contents in the nanocomposite (Fig. S7). The HRTEM images shown in Figure 6 and S8 reveal different orientations and interplanar spacing and show lattice fringes for TiO_2 and Cu_{2-x}Se contents. In particular, an interplanar distance of 0.209 nm could be attributed to the (202) plane of Cu_{2-x}Se , as also confirmed by the selected area diffraction pattern (Fig. 6d).

c) Photocatalysis

Using the $\text{Cu}_{2-x}\text{Se-TiO}_2$ nanocomposites as photocatalysts, we performed photodegradation studies on FA solution under UV and visible light by monitoring with HPLC. Figure S9 presents the experimental setting for the photocatalytic degradation of FA, where a 100 mL photoreactor was used. All samples were stirred for 30 minutes in dark to reach the adsorption-desorption equilibrium. While no significant difference in the adsorption of formic acid was observed, the nanocomposite samples with 0.1% and 0.3mol% of copper selenide exhibited enhanced photocatalytic activities vis-à-vis pure TiO_2 . For these samples, FA was completely degraded within 45 minutes under UV radiation. This improved efficiency of the $\text{TiO}_2\text{-Cu}_{2-x}\text{Se}$ nanocomposites can be attributed to an enhanced light absorption property and an increased separation of e^-h^+ pairs in these composites (Fig. S10), as also noted previously.^{6,38} This charge transfer process is thermodynamically favored as both the conduction band and the valence band of Cu_{2-x}Se lie above that of TiO_2 , and the e^-h^+ transfer process is faster than its recombination.⁹ The $\text{Cu}_{2-x}\text{Se-TiO}_2$ nanocomposite generates e^-h^+ pairs when irradiated with UV-visible light (eqn S1-2 in the Supporting Information). On one hand, electrons produced reacts with adsorbed oxygen molecules to form superoxide radicals ($\text{O}_2^{\cdot-}$), the positively charged holes (h^+), on the other hand, generate HCOO^{\cdot} radical upon reaction with HCOOH dissolved in H_2O (eqn S3-4 in the Supporting Information). These are consistent with previous observations.³⁹ Formic acid then gives CO_2 , while

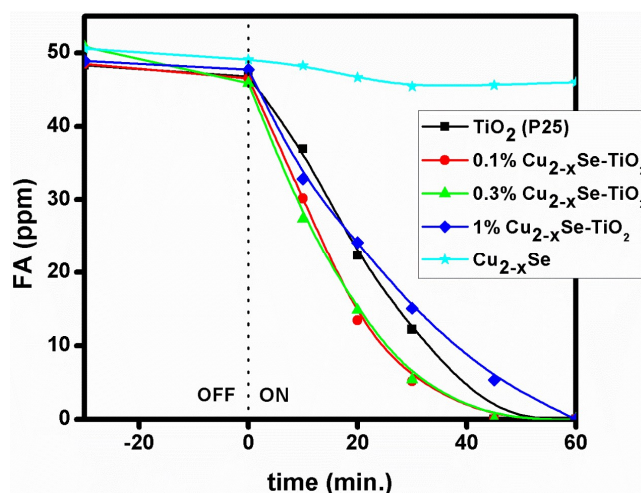


Figure 7. Photodegradation of FA using TiO_2 , Cu_{2-x}Se and $\text{Cu}_{2-x}\text{Se-TiO}_2$ with different % of Cu_{2-x}Se under UV light.

$\text{O}_2^{\cdot-}$ combines with H^+ to generate HO_2^{\cdot} (eqn S5-6 in the Supporting Information). Previous studies have reported the two-step catalytic degradation of formic acid: first to formate and then to CO_2 .⁴⁰ The composite with 1% Cu_{2-x}Se content, however, showed reduced activity. We can correlate this to the fact that a high content of copper selenide darkens the sample, which leads to an insufficient usage of UV radiations and a lower number of electron-hole pairs. An initial attempt to degrade FA using $\text{Cu}_{2-x}\text{Se-TiO}_2$ nanocomposites under visible light was ineffective, and no activity was observed (Figure S11). Even though the band gap for the composites reported here is reduced and visible light absorption is improved, it may not be enough to bring the changes for the visible lamp we used (which emits photons only after 410 nm). It is also quite possible that the absorbed photons are used for some other reactions such as producing heat or emitting fluorescence or the generated e^- and h^+ are recombined rapidly.² We are currently trying to understand the synergistic effect between Cu_{2-x}Se & TiO_2 components and establish a thorough mechanism by employing different experimental conditions (power and position of the lamp, filters used, stirring speed, formic acid concentration...). These as-prepared photocatalysts can be recycled with only a slight decrease in the activity (Fig. S12). To test the chemical stability of the catalysts, we carried out blank photocatalytic experiments using water and acidic water (HNO_3 , pH = 3.68, 26 °C) in place of formic acid under UV radiation. We observed no significant peak of any organic molecule from HPLC results, thus conforming that these catalysts remain chemically stable during photocatalytic experiments (Fig. S13).

Conclusions

Divergent reactivity of $t\text{-Bu}_2\text{Se}$ with copper reagents is presented. It includes direct synthesis of copper selenide nanoparticles from the reaction of ditertiarybutyl selenide ($t\text{-Bu}_2\text{Se}$) and copper(II) trifluoroacetate [$\text{Cu}(\text{TFA})_2$]. Successful isolation and characterization of an intermediate molecular species [$\text{Cu}_2(\text{TFA})_2(t\text{-Bu}_2\text{Se})_3$] during the course of this reaction established unequivocally the route for the formation of copper

selenide nanoparticles. The mild conditions required to get these narrow-band gap semiconducting Cu_{2-x}Se NPs offered an easy synthesis of *n*%Cu_{2-x}Se-TiO₂ nanocomposites with different Cu/Ti ratios, among which *n* = 0.1 and 0.3 mol% showed improved photocatalysis in comparison to the commercial available TiO₂ (P25) for the formic acid degradation under UV irradiation. Additional studies are currently underway to optimize the synthetic and experimental conditions to improve further the photocatalytic activity of these nanocomposites.

Conflicts of interest

There are no conflicts of interest to declare.

Acknowledgements

SG thanks the French ministry of higher education, research and innovation for her PhD grant (doctoral school of chemistry, Lyon). Authors also thank M. Aouine and L. Burel (electron microscopic measurements), Dr. L. Cardenas (XPS), Y. Aizac (PXRD) and P. Mascunan (BET measurements) of IRCELYON. We are grateful to Prof. S. Daniele for his constant encouragement.

Notes and references

^a Univ Lyon, Université Claude Bernard Lyon 1, CNRS, IRCELYON-UMR 5256, 2 avenue Albert Einstein, 69626 Villeurbanne, France

^b Univ Lyon, Université Claude Bernard Lyon 1, Centre de Diffraction Henri Longchambon, 5 rue de La Doua, 69100 Villeurbanne, France

S. M.: e-mail, shashank.mishra@ircelyon.univ-lyon1.fr. Fax: 33-472445399; Tel: 33 472445322.

† Electronic Supplementary Information (ESI) available: Powder XRD, SEM, STEM, TEM and EDX of Cu_{2-x}Se and Cu_{2-x}Se-TiO₂ composites obtained under different conditions, experimental setup and graphical plots of photodegradation of formic acid by Cu_{2-x}Se-TiO₂ and recycled catalysts under UV-visible region. CCDC 1835505-1835506 contain the supplementary crystallographic data for this article. These data can be obtained free of charge from the Cambridge Crystallographic Data Centre. For ESI and crystallographic data in CIF or other electronic format see DOI: 10.1039/b000000x/.

- R. Dagherira, P. Droguia and D. Robertb, *J. Photochem. Photobiol. A Chem.*, 2012, **238**, 41–52.
- M. Kapilashrami, Y. Zhang, Y.-S. Liu, A. Hagfeldt and J. Guo, *Chem. Rev.*, 2014, **114**, 9662–9707.
- Y. Liu, P. Zhang, B. Tian and J. Zhang, *Catal. Commun.*, 2015, **70**, 30–33.
- J. Lee, T. G. Kim, H. Choi and Y. Sung, *Cryst. Growth Des.*, 2007, **7**, 2588–2593.
- Z. Hana, L. Ren, M. Luo, L. Chen, H. Pan, C. Li, J. Chen and J. Lan, *J. Mol. Catal. A: Chem.*, 2016, **425**, 229–236.
- W. L. Ong, Y. Lim, J. L. T. Ong and G. W. Ho, *J. Mater. Chem. A.*, 2015, **3**, 6509–6516.
- S. Mishra, D. Du, E. Jeanneau, F. Dappozze, C. Guillard, J. Zhang and S. Daniele, *Chem. Asian J.*, 2016, **11**, 1658–1663.
- B. Chong, W. Zhu, Y. Liu, L. Guan and G. Z. Chen, *J. Mater. Chem. A.*, 2016, **4**, 1336–1344.
- C. Coughlan, M. Ibáñez, O. Dobrozhan, A. Singh, A. Cabot and K. Ryan, *Chem. Rev.*, 2017, **117**, 5865–6109.
- D. Chen, G. Chen, R. Jinb and H. Xua, *CrystEngComm*, 2014, **16**, 2810–2817.
- D. Li, Z. Zheng, Y. Lei, S. Ge, Y. Zhang, Y. Zhang, K. Wong, F. Yanga and W. Lau, *CrystEngComm*, 2010, **12**, 1856–1861.
- X. Liu, X. Duan, P. Penga and W. Zheng, *Nanoscale*, 2011, **3**, 5090–5095.
- L. Zhu, Y. Zhao, W. Zheng, N. Ba, G. Zhang, J. Zhang, X. Li, H. Xiea and L. Bie, *CrystEngComm*, 2016, **18**, 5202–5208.
- S. Q. Lie, D. M. Wang, M. X. Gaoa and C. Z. Huang, *Nanoscale*, 2014, **6**, 10289–10296.
- G. Tian, T. Zhao, J. Niu, H. Shen and L. S. Lia, *RSC Adv.*, 2014, **4**, 39547–39551.
- W. Wang, L. Zhang, G. Chen, J. Jiang, T. Ding, J. Zuo and Q. Yang, *CrystEngComm*, 2015, **17**, 1975–1981.
- (a) S. Mishra and S. Daniele, *Chem. Rev.*, 2015, **115**, 8379–8448; (b) K. Soussi, S. Mishra, E. Jeanneau, J.-M. M. Millet and S. Daniele, *Dalton Trans.*, 2017, **46**, 13055–13064; (c) S. Mishra, E. Jeanneau, M. Rolland and S. Daniele, *RSC Adv.*, 2016, **6**, 1738–1743; (d) S. Mishra, E. Jeanneau, S. Mangematin, H. Chermette, M. Poor Kalhor, G. Bonnefont, G. Fantozzi, S. Le Floch, S. Pailhes and S. Daniele, *Dalton Trans.*, 2015, **44**, 6848–6862; (e) S. Mishra, V. Mendez, E. Jeanneau, V. Caps and S. Daniele, *Eur. J. Inorg. Chem.*, 2013, 500–510; (f) S. Mishra, E. Jeanneau, M.-H. Berger, J.-F. Hocheplid and S. Daniele, *Inorg. Chem.*, 2010, **49**, 11184–11189; (g) S. Mishra, E. Jeanneau, S. Daniele and V. Mendez, *Dalton Trans.*, 2010, **39**, 7440–7443.
- (a) H. Lu and R. L. Brutchey, *Chem. Mater.*, 2017, **29**, 1396–1403; (b) S. Gupta, H. Joshi, N. Jain and A. K. Singh, *J. Mol. Catal. A: Chem.*, 2016, **423**, 135–142; (c) R. K. Sharma, G. Kedarnath, V. K. Jain, A. Wadawale, C. G. S. Pillai, M. Nalliath and B. Vishwanadh, *Dalton Trans.*, 2011, **40**, 9194–9201; (d) M. Afzaal, M. A. Malik and P. O'Brien, *J. Mater. Chem.*, 2010, **20**, 4031–4040.
- (a) Y.-P. Chang, A. L. Hector, W. Levason, G. Reid and J. Whittam, *Dalton Trans.*, 2018, **47**, 2406–2414; (b) C. Gurnani, S. L. Hawken, A. L. Hector, R. Huang, M. Jura, W. Levason, J. Perkins, G. Reid and G. B. G. Stenning, *Dalton Trans.*, 2018, **47**, 2628–2637; (c) Y.-P. Chang, A. L. Hector, W. Levason and G. Reid, *Dalton Trans.*, 2017, **46**, 9824–9832; (d) K. George, C. H. de Groot, C. Gurnani, A. L. Hector, R. Huang, M. Jura, W. Levason and G. Reid, *Chem. Mater.*, 2013, **25**, 1829–1836; (e) S. L. Benjamin, C. H. de Groot, C. Gurnani, A. L. Hector, R. Huang, K. Ignatyev, W. Levason, S. J. Pearce, F. Thomas and G. Reid, *Chem. Mater.*, 2013, **25**, 4719–4724; (f) C. H. de Groot, C. Gurnani, A. L. Hector, R. Huang, M. Jura, W. Levason and G. Reid, *Chem. Mater.*, 2012, **24**, 4442–4449; (g) A. L. Hector, M. Jura, W. Levason, S. D. Reid and G. Reid, *New J. Chem.*, 2009, **33**, 641–645;
- (a) J. R. Sparks, R. He, N. Healy, M. Krishnamurthi, A. C. Peacock, P. J. Sazio, V. Gopalan and J. V. Badding, *Adv. Mater.*, 2011, **23**, 1647–1651; (b) N. D. Boscher, C. J. Carmalt, R. G. Palgrave and I. P. Parkin, *Thin Solid Films*, 2008, **516**, 4750–4757; (c) N. D. Boscher, C. J. Carmalt, G. Hyett, A. G. Prieto, Q. A. Pankhurst and I. P. Parkin, *J. Mater. Chem.*, 2008, **18**, 1667–1673; (d) N. D. Boscher, C. J. Carmalt and I. P. Parkin, *J. Mater. Chem.*, 2006, **16**, 122–127; (e) N. D. Boscher, C. J. Carmalt, R. G. Palgrave, J. J. Gil-Tomas and I. P. Parkin, *Chem. Vap. Deposition*, 2006, **12**, 692–698; (f) N. D. Boscher, C. J. Carmalt and I. P. Parkin, *Eur. J. Inorg. Chem.*, 2006, 1255–1259.
- (a) K. Ramasamy, M. A. Malik, N. Revaprasadu and P. O'Brien, *Chem. Mater.* 2013, **25**, 3551–3569; (b) M. Afzaal, M. A. Malik and P. O'Brien, *J. Mater. Chem.* 2010, **20**, 4031–4040.
- A. Turki, C. Guillard, F. Dappozze, G. Berhault, Z. Ksibi and H. Kochkar, *J. Photochem. Photobiol. Chem.* 2014, **279**, 8–16.
- CrysAlisPro, Agilent Technologies, Version 1.171.34.49 (release 20-01-2011 CrysAlis171.NET) (compiled Jan 20 2011, 15:58:25).
- R. C. Clark and J. S. Reid, *Acta Cryst. A*, 1995, **51**, 887–897.
- A. Altomare, M. C. Burla, M. Camalli, G. L. Casciarano, C. Giacovazzo, A. Guagliardi, A. G. G. Moliterni, G. Polidori and R. Spagna, *J. App. Cryst.*, 1999, **32**, 115–119.
- P. W. Betteridge, J. R. Carruthers, R. I. Cooper, K. Prout and D. J. Watkin, *J. Appl. Cryst.*, 2003, **36**, 1487.
- A. L. Hector, M. Jura, W. Levason, S. D. Reid and G. Reid, *New J. Chem.*, 2009, **33**, 641–645.
- A. C. Jones and M. L. Hitchman, Chemical Vapour Deposition: Precursors, Processes and Applications, Royal Society of Chemistry, 2009.
- S. Mishra, E. Jeanneau and S. Daniele, *Polyhedron*, 2010, **29**, 500–506.

- 30 (a) W. Ji, J. Qu, C.-A. Li, J.-W. Wu, S. Jing, F. Gao, Y.-N. Lv, C. Liu, D.-R. Zhu, X.-M. Ren and W. Huang, *Appl. Catal. B: Environ.*, 2017, **205**, 368–375; (b) W. Ji, J. Qu, S. Jing, D. Zhu and W. Huang, *Dalton Trans.*, 2016, 45, 1016–1024; (c) Y.-Q. Liu, W. Ji, H.-Y. Zhou, Y. Li, S. Jing, D.-R. Zhu and J. Zhang, *RSC Adv.*, 2015, **5**, 42689–42697; (d) A. Panda, *Coord. Chem. Rev.*, 2009, **253**, 1056; (e) W. Levason, S. Orchard and G. Reid, *Coord. Chem. Rev.*, 2002, **225**, 159; (f) M. Knorr, A. Bonnot, A. Lapprand, A. Khatyr, C. Strohmman, M. M. Kubicki, Y. Rousselin and P. D. Harvey, *Inorg. Chem.*, 2015, **54**, 4076–4093.
- 5 31 (a) Y. Chen, S. Mishra, G. Ledoux, E. Jeanneau, M. Daniel, J. Zhang and S. Daniele, *Chem. Asian J.*, 2014, **9**, 2415–2421; (b) S. Mishra, E. Jeanneau, A.-L. Bulin, G. Ledoux, B. Jouguet, D. Amans, A. Belsky, S. Daniele and C. Dujardin, *Dalton Trans.*, 2013, **42**, 12633–12643; (c) S. Mishra, L. G. Hubert-Pfalzgraf, S. Daniele, M. Rolland, E. Jeanneau and B. Jouguet, *Inorg. Chem. Commun.*, 2009, **12**, 97–100.
- 10 32 (a) S. Mishra, E. Jeanneau, G. Ledoux and S. Daniele, *Inorg. Chem.*, 2014, **53**, 11721–11731; (b) S. Mishra, E. Jeanneau, G. Ledoux and S. Daniele, *CrystEngComm*, 2012, **14**, 3894–3901; (c) S. Mishra, E. Jeanneau, S. Daniele and L. G. Hubert-Pfalzgraf, *CrystEngComm*, 2008, **10**, 814–816.
- 15 33 M. Knorr, A. Pam, A. Khatyr, C. Strohmman, M. M. Kubicki, Y. Rousselin, S. M. Aly, D. Fortin and P. D. Harvey, *Inorg. Chem.* 2010, **49**, 5834–5844.
- 20 34 S. Mishra, J. Zhang, L. G. Hubert-Pfalzgraf, D. Luneau and E. Jeanneau, *Eur. J. Inorg. Chem.*, 2007, 602–608.
- 25 35 W. Ji, J. Qu, C.-A. Li, J.-W. Wu, S. Jing, F. Gao, Y.-N. Lv, C. Liu, D.-R. Zhu, X.-M. Ren and W. Huang, *Appl. Catal. B: Environ.* 2017, **205**, 368–375.
- 30 36 (a) B. Bhattacharyya and A. Pandey, *J. Am. Chem. Soc.*, 2016, **138**, 10207–10213; (b) Y.-J. Yuan, G. Fang, D. Chen, Y. Huang, L.-X. Yang, D. Cao, J.-J. Wang, Z. T. Yu and Z. Zou, *Dalton Trans.*, 2018, **47**, 5652–5659.
- 35 37 W. Ou, Y. Zou, K. Wang, W. Gong, R. Pei, L. Chen, Z. Pan, D. Fu, X. Huang, Y. Zhao, W. Lu and J. Jiang, *J. Phys. Chem. Lett.*, 2018, **9**, 274–280.
- 38 A. Turki, H. Kochkar, C. Guillard, G. Berhault and A. Ghorbel, *Appl. Catal. B.*, 2013, **138–139**, 401–415.
- 39 A. Hamandi, G. Berhault, C. Guillard and H. Kochkar, *Mol. Catal.* 2017, **432**, 125–130.
- 40 40 M. F. J. Dijkstra, H. J. Panneman, J. G. M. Winkelman, J. J. Kelly and A. A. C. M. Beenackers, *Chem. Eng. Sci.*, 2002, **57**, 4895–4907.

Graphical Abstract

Precursor-mediated synthesis of Cu_{2-x}Se nanoparticles and its nanocomposites with TiO_2 for improved photocatalysis

S. Gahlot, E. Jeanneau, F. Dappozze, C. Guillard and S. Mishra*

Simple, but effective. Successful isolation and characterization of an intermediate during the reaction of $t\text{-Bu}_2\text{Se}$ with $\text{Cu}(\text{TFA})_2$ establishes the route for the formation of copper selenide NPs and $\text{Cu}_{2-x}\text{Se}-\text{TiO}_2$ composites as active photocatalysts.

